CONF-860421--30

# MICROSTRUCTURAL EVOLUTION IN AN AUSTENITIC STAINLESS STEEL FUSION REACTOR FIRST WALL*

CONF-860421--30

DE86 010395

R. E. Stoller† and G. R. Odette††

†Metals and Ceramics Division, Oak Ridge National Laboratory,
P. O. Box X, Oak Ridge, TN 37831

††Department of Chemical and Nuclear Engineering
University of California
Santa Barbara, CA 93106

ABSTRACT

Near-term fusion reactors will have to be designed using radiation effects data from experiments conducted in fast fission reactors. These fast reactors generate atomic displacements at a rate similar to that expected in a DT fusion reactor first wall. However, the transmutant helium production in an austenitic stainless steel first wall will exceed that in fast reactor fuel cladding by about a factor of 30. Hence, the use of the fast reactor data will involve some extrapolation. A major goal of this work is to develop theoretical models of microstructural evolution to aid in this extrapolation.

In the present work a detailed rate-theory-based model of microstructural evolution under fast neutron irradiation has been developed. The prominent new aspect of this model is a treatment of dislocation evolution in which Frank faulted loops nucleate, grow and unfault to provide a source for network dislocations while the dislocation network can be simultaneously annihilated by a climb/glide process. The predictions of this model compare very favorably with the observed dose and temperature dependence of these key microstructural features over a broad range. This new

*Research sponsored by the Office of Fusion Energy, U.S. Department of Energy, under contract DE-AC05-840R21400 with Martin Marietta Energy Systems, Inc. and contract AM03-76SF0034 with University of California, Santa Barbara.

description of dislocation evolution has been coupled with a previously developed model of cavity evolution and good agreement has been obtained between the predictions of the composite model and fast reactor swelling data as well. The results from the composite model also reveal that the various components of the irradiation-induced microstructure evolve in a highly coupled manner. The predictions of the composite model are more sensitive to parametric variations than more simple models. Hence, its value as a tool in data analysis and extrapolation is enhanced.

## INTRODUCTION

During the last 10 to 15 years, a large amount of radiation effects data has been produced. The focus of much of this experimental effort has been to increase our understanding of void swelling and microstructural evolution in austenitic stainless steels. Almost all of these experiments have been carried out in fast fission reactors where the damage rate is similar to that which will occur in the first wall of a fusion reactor fueled by deuterium and tritium (DT). Unfortunately, the production of helium by transmutation reactions in an austenitic stainless steel fusion reactor first wall will be about 30 times greater than the value obtained in fast reactor irradiations. This difference is most conveniently expressed as the ratio of transmutant helium to atomic displacements (He/dpa ratio). The He/dpa ratio is about 0.35 appm He/dpa in the Experimental Breeder Reactor-II (EBR-II) and will be about 10 appm He/dpa in a DT fusion reactor first wall. Therefore, the use of this fast reactor data to design near-term fusion reactors will require some extrapolation.

One purpose of the work discussed below is to aid this extrapolation by developing theoretical models of microstructural evolution under fast neutron irradiation. These models can be used in the analysis of irradiation experiments to identify key mechanisms and parameters for further study. The use of fast reactor data to calibrate such models also permits them to be used in a predictive fashion. Earlier work has involved the use of more simple cavity evolution models in just this way (1–4). A major limitation of the work just referenced was the neglect of the dose dependence of microstructural features other than the cavities. The present work represents an effort to remove this limitation by generating in a self-consistent manner the time dependence of the major microstructural features observed in irradiated stainless steels; cavities, Frank faulted dislocation loops and network dislocations. The influence of second phase precipitate particles is included to a limited degree as described previously (4). The model does not yet include any explicit treatment of microchemical evolution. The specific values of the various rate-theory parameters used to calibrate the model can approximately account for this neglect. The major approximation in this case is that the value of parameters which can be altered by microchemical evolution (e.g. point defect biases and diffusivities) are essentially time-averaged.

## MODEL DESCRIPTION

Because the details of the model are discussed elsewhere (5,6), only a summary description of the model's features will be given here. The present work is an extension of the cavity evolution models referenced above

(1–4). That work helped to establish a generally accepted sequence of events which leads to void formation in irradiated stainless steels. Voids are believed to form as the result of gas-stabilized bubbles reaching a critical size beyond which additional gas is not required for growth. This critical size is determined primarily by the matrix free surface energy, the temperature and the vacancy supersaturation (7). References 4 and 7 describe the aspects of the model which concern cavity evolution in detail.

The familiar rate theory approach (4,11) is used to compute the sink strengths of the various extended defects and the point defect concentrations. The concentration of vacancies and mono-, di-, tri- and tetra-interstitials are computed at quasi-steady-state. Only the mono-defects are considered to be mobile (12). The tetra-interstitial is assumed to be a stable nucleus for Frank faulted loop growth. The model includes the following extended defects: bubbles, voids, transient vacancy clusters in the form of microvoids, subgrain structure, Frank faulted loops and network dislocations. The faulted loops and network dislocations are assigned a bias for interstitials; all other sinks are unbiased.

The consideration of small interstitial clusters modifies the conventional equations for the vacancy and interstitial concentrations by including terms which reflect their loss due to impingement upon such clusters. The equations for the di- and tri-interstitial clusters reflect growth and shrinkage by reactions with the mono-defects (5,6). The equation describing the tetra-interstitial population provides a transition between the discrete cluster regime and the Frank faulted loop regime. This

"hybrid" equation describes single atom transitions between the tri- and tetra-interstitial but uses an effective transition time to describe losses to the larger loop population,

$$\frac{dC_4}{dt} = \beta_i^3 C_3 - \beta_v^4 C_4 - C_4 \tau_4^{-1} \tag{1}$$

The $\beta_{i,v}^j$ terms in Eq. (1) are impingement rates of the mono-defects on the j-th cluster size (5,6). The $\tau_4$ term in Eq. (1) is the lifetime of a tetra-interstitial against growth to the size of the first loop size class, $r_1^\ell$. If $r_4$ is the radius of the tetra-interstitial,

$$\tau_4 = \int_{r_4}^{r_1^\ell} \left(\frac{dr_\ell}{dt}\right)^{-1} dr_\ell \tag{2}$$

in which $dr_\ell/dt$ is the loop growth rate. The loop population is described by equations of the form:

$$\frac{dN_i^\ell}{dt} = N_{i-1}^\ell \tau_i^{-1} - N_i^\ell \tau_{i+1}^{-1} \tag{3}$$

where $N_i^\ell$ is the number of loops in a given size class with radius $r_i^\ell$ and the $\tau_i$ are computed with appropriate limits using Eq. (2).

Equation (1) has been shown to provide an adequate boundary condition between the two regions in which alternate mathematical descriptions of interstitial loop growth (5,6). The use of the discrete clustering description would require greater than $10^4$ equations to describe the loop population. The hybrid description requires about 20.

The model for the evolution of the network dislocations includes four components, two of which are only active under irradiation while the other two are thermally activated. The thermal components are a high temperature climb source term due to Bardeen-Herring sources and an annihilation term due to stress-assisted directional diffusion of vacancies. The development of these components owes much to similar models which have been developed in the study of creep (13,14). The Bardeen-Herring sources for network dislocations are similar to Frank-Read sources except that the latter are glide driven while the former are climb driven (15). A simple geometrical argument leads to a network dislocation ($\rho_n$) generation rate from Bardeen-Herring sources (5,6):

$$R_{th}^{\rho_n} = 2\pi v_{cl}^{\sigma} S_D \tag{4}$$

in which $v_{cl}^{\sigma}$ is the dislocation climb velocity in the presence of a back stress due to pinned dislocations (16,17) and $S_D$ is the source density. Network dislocations can also be annihilated when segments with opposite Burgers vectors climb together. If the average climb distance to annihilation is $d_{cl}$, the characteristic time for this process is:

$$\tau_{th} = \frac{d_{cl}}{v_{cl}^{\sigma}} . \tag{5}$$

Under irradiation the unfaulting of Frank loops provides an additional source of network dislocations. The model assumes that the maximum faulted loop size is governed by the geometric constraint that the loop unfaults

upon contacting another loop or network dislocation. This leads to an unfaulting radius

$$r_{unf}^{\ell} = (\pi\rho_t)^{-1/2} \tag{6}$$

in agreement with observation (18). In Eq. (6) $\rho_t$ is the total dislocation density. The rate at which loops unfault ($\tau_{unf}^{-1}$) is calculated using Eq. (2). Finally, bias driven climb under irradiation can also lead to the annihilation of network dislocations. The climb velocity in this case is:

$$v_{cl}^{irr} = \frac{1}{b}\left[Z_i^n D_i C_i - Z_v^n D_v (C_v - C_v^n)\right] . \tag{7}$$

The characteristic time for this process is given by analogy with Eq. (5) and the two lifetimes are added using an electrical resistance analog:

$$\tau_T = (\tau_{irr}^{-1} + \tau_{th}^{-1})^{-1} \quad . \tag{8}$$

This leads to the rate equation describing the evolution of the dislocation network as

$$\frac{d\rho_n}{dt} = 2\pi(v_{cl}^{\sigma} S_D + r_{unf}^{\ell} N_{unf}^{\ell} \tau_{unf}^{-1}) - \rho_n \tau_T^{-1} . \tag{9}$$

## MODEL CALIBRATION AND PREDICTIONS

Such a complex microstructural model includes a number of physical parameters. Unfortunately, values for many of the required parameters are not well known or have only been measured in pure materials. Because of

this uncertainty about parameter values, the predictions of even a well calibrated model may not be based on a unique set of parameter values. Other combinations of parameters can give very similar results. One goal of the present work was to try to limit the range of possible parameter choices by including additional physical mechanisms in a well understood, simple model. This has proven to be successful. A full description of the model calibration can be found in References 5 and 6, a couple of examples of this work will be given here.

The thermal dislocation evolution model was first calibrated by predicting the recovery of 20% cold-worked material with the dose rate set to zero. Using reasonable values of model parameters, very good agreement was obtained with dislocation densities in 20% cold-worked and aged AISI 316 stainless steel (5,6,19,20). Then the swelling predictions of the model were calibrated using swelling data from irradiations in the EBR-II of several heats of AISI 316 stainless steel which had been developed for the first core of the Fast Flux Test Facility (FFTF) (21,22). These so-called FFTF first core heats were chosen to minimize the effect of heat-to-heat variations. Figure 1 compares the predicted swelling and the first core data at an intermediate and high fluence. The model predicts both similar incubation times and peak swelling rates. Figure 2 and Fig. 3 compare the predicted network dislocation density and peak Frank faulted loop density with fast reactor data from several sources (18,20,23–27). Here again the agreement is very good.

An example of a new parametric dependence in the model is shown in Fig. 4, a–c. Here the influence of the interstitial migration energy on the swelling, network dislocation density and peak faulted loop density is shown. The curves labeled as the base case use $E_i^m = 0.85$. The results of the simple void swelling theory are not sensitive to this parameter (28) and a much lower value (<0.5 eV) which reflects measurements on pure materials is normally used (1–4,29). However the present model is sensitive to $E_i^m$ via its effect on the loop population. The loop evolution in turn influences the network dislocation density and the predicted swelling. An analysis of Fig. 4, a–c reveals the complex coupling of the evolution of these three microstructural features. The higher interstitial migration energy is also consistent with recent measurements of this parameter in austenitic stainless steels (30,31).

During the calibration, the model was also used to compare alternate descriptions of the faulted loop/interstitial bias, $Z_i^\ell$. If interstitial absorption at faulted loops is diffusion limited, a size dependent bias is obtained (32) while if the absorption is reaction rate limited a constant loop bias would result. The temperature dependence of the predicted faulted loop density at 50 and 100 dpa and the peak loop density are shown in Fig. 5. The size dependent used bias was that of Wolfer and Ashkin (32). The maximum value of $Z_i^\ell(r_\ell)$ was 3.5 for the smallest loops and it asymptotically approached the network dislocation/interstitial bias at large sizes. The results for a constant loop bias in Fig. 5 reflect a value of 1.50. The predictions using the size dependent bias are clearly too high at the higher temperatures. This result is in agreement with an

analysis of loop growth during electron irradiation performed by Yoo and Stiegler (33).

## MODEL EXTRAPOLATION TO FUSION CONDITIONS

The calibrated model has been used to predict swelling in a DT fusion reactor first wall. The predictions were made for an increased He/dpa ratio of 10 appm He/dpa. The most systematically observed trend in the literature on helium effects is that higher He/dpa ratios promote cavity formation (34,35). The effect can be approximately described by a simple power dependence of the cavity density, $N_c$, on the He/dpa ratio

$$N_c \alpha (\text{He/dpa})^p \ , \tag{10}$$

where p is typically in the range of 0.5–1 (34). Here we have scaled the initial bubble densities up from the fast reactor values using Eq. (10) with values of p reflecting weak (p = 0.2) to fairly strong (p = 0.8) dependence on the He/dpa ratio.

Figure 6 shows the predicted swelling and network dislocation density for an intermediate value of p, p = 0.5. The general trends include a reduced incubation time at all temperatures and enhanced swelling at both low and high temperatures at high doses for the fusion case. At intermediate temperatures and high doses the predicted swelling for fusion is less than the fast reactor value due to a reduced swelling rate. The dislocation density is generally somewhat lower than for the fusion He/dpa ratio. There is some support for this prediction in the reported dislocation densities for one heat of AISI 316 stainless steel which has been irradiated in both the EBR-II (~0.35 appm He/dpa) and the High Flux Isotope

Reactor (~70 appm He/dpa) (36). The explicit dependence of swelling on cavity density is shown in Fig. 7. The details of the behavior are complex due to the interactions between the various defect types but the trends observed in Fig. 6 are maintained.

The reduced incubation times and enhanced low temperature swelling have potentially significant implications for fusion reactor designs. Only a very limited amount of dimensional instability can be accommodated in typical reactor designs (37,38) hence the incubation time is perhaps a parameter of more engineering significance than the peak swelling rate. Further, recent conceptual designs using austenitic stainless steels have tended to move toward lower operating temperatures (37,38).

## SUMMARY

The use of a comprehensive rate-theory model of microstructural evolution under fast neutron irradiation has been described. The new features of this model include an explicit treatment of the dose dependence of both Frank faulted loops and network dislocations. The more complex model has been shown to provide a powerful analytical tool for data analysis and the evaluation of various theoretical concepts. Because the model includes additional physical mechanisms, it is more sensitive to arbitrary parameter changes. This "stiffness" is believed to be physically meaningful.

The new model was calibrated using a well defined set of fast reactor swelling data. The calibrated model was then used to predict swelling in an austenitic stainless steel fusion reactor first wall. The predictions

indicate that fast reactor swelling data may not provide an adequate representation of swelling in a fusion reactor. Specifically, low temperature swelling is enhanced and incubation times are reduced at all relevant temperatures for fusion reactor conditions. These results highlight the need for additional theoretical and experimental work to improve our understanding of helium effects in a fast neutron irradiation environment. A recently proposed set of experiments involving the use of isotopically tailored alloys to obtain a range of He/dpa ratios in a single reactor should be particularly useful (39,40).

REFERENCES


1. G. R. Odette and S. C. Langley, Radiation Effects and Tritium Technology for Fusion Reactors, CONF-750989, 1975, I: 395–416.
2. R. E. Stoller and G. R. Odette, J. Nucl. Mater. 103–104 (1981) 1361–1365.
3. G. R. Odette and R. E. Stoller, J. Nucl. Mater. 122&123 (1984) 514–519.
4. R. E. Stoller and G. R. Odette, "The Effect of Helium on Swelling in Stainless Steel: Influence of Cavity Density and Morphology," Effects of Radiation on Materials: Eleventh Int. Symp., ASTM STP 782, ASTM, 1982, 275–294.
5. R. E. Stoller and G. R. Odette, "A Composite Model of Microstructural Evolution in Austenitic Stainless Steel Under Fast Neutron Irradiation," Effects of Radiation on Materials: Thirteen Int. Symp., Chicago, Ill., June 23–25, 1986, to be published by the American Society for Testing and Materials.
6. R. E. Stoller and G. R. Odette, Damage Analysis and Fundamental Studies, Quarterly Progress Report, DOE/ER-0046/23, November, 1985, 34–48.
7. R. E. Stoller and G. R. Odette, J. Nucl. Mater. 131 (1985) 118–125.
8. L. K. Mansur and W. A. Coghlan, J. Nucl. Mater. 119 (1983) 1–25.
9. M. R. Hayns, The Transition From Gas Bubble to Void Growth, AERE-R8806, U.K.A.E.A., 1977.
10. K. C. Russell, Acta Met. 26 (1978) 1615–1630.
11. A. D. Brailsford and R. Bullough, The Theory of Sink Strengths, AERE Harwell Report TP.854, 1980.
12. R. A. Johnson, J. Nucl. Mater. 83 (1979) 147–159.

13. F. R. N. Nabarro, Phil. Mag. 16 (1967) 231–237.

14. J. Gittus, Creep, Viscoelasticity and Creep Fracture in Solids, John Wiley and Sons, New York, 1975.

15. J. Bardeen and C. Herring, Imperfections in Nearly Perfect Crystals, W. Schockley (Ed.), John Wiley and Sons, New York, 1952.

16. W. D. Nix, R. Gasca-Neri, and J. P. Hirth, Phil. Mag. 23 (1971) 1339–1349.

17. G. B. Gibbs, Phil. Mag. 23 (1971) 771–780.

18. H. R. Brager, F. A. Garner, and G. L. Guthrie, J. Nucl. Mater. 66 (1977) 181–197.

19. D. Fahr, E. E. Bloom, and J. O. Stiegler, "Irradiation Embrittlement and Creep in Fuel Cladding and Core Components," Proc. of BNES Conf., London, 1972, 167–177.

20. P. J. Maziasz, Alloy Development for Irradiation Performance, Quarterly Progress Report, DOE/ER-0045/7, September, 1981, 54–97.

21. J. F. Bates and M. K. Korenko, Nucl. Tech. 48 (1980) 303–314.

22. F. A. Garner, "Overview of the Swelling Behavior of 316 Stainless Steel," Optimizing Materials for Nuclear Applications, Symp. Proc., TMS AIME, New York, 1985.

23. J. I. Bramman, C. Brown, J. S. Watkin, C. Cawthorne, E. J. Fulton, P. J. Barton, and E. A. Little, "Void Swelling and Microstructural Changes in Fuel Pin Cladding and Unstressed Specimens Irradiated in DFR," Radiation Effects in Breeder Reactor Structural Materials, Int. Conf. TMS AIME, New York, 1977, 479–507.

24. E. E. Bloom and J. O. Stiegler, Effects of Irradiation on Substructure and Mechanical Properties of Metals and Alloys, ASTM STP 529, ASTM, 1973, 360–382.

25. H. R. Brager and J. L. Straalsund, J. Nucl. Mater. 46 (1973) 124–158.

26. P. J. Barton, B. L. Eyre, and D. A. Stow, J. Nucl. Mater. 67 (1977) 181–197.

27. H. R. Brager, J. Nucl. Mater. 57 (1975) 103–118.

28. L. K. Mansur, J. Nucl. Mater. 83 (1979) 109–127.

29. F. W. Young, J. Nucl. Mater. 69&70 (1978) 310–370.

30. O. Dimitrov and C. Dimitrov, J. Nucl. Mater. 105 (1982) 39–47.

31. J. T. Stanley and J. R. Cost, J. Phys. F: Met. Phys. 14 (1984) 1801–1810.

32. W. G. Wolfer and M. Ashkin, J. Appl. Phys. 46 (1975) 547–557 and erratum.

33. M. H. Yoo and J. O. Stiegler, Phil. Mag. 36 (1977) 1305–1315.

34. G. R. Odette, P. J. Maziasz and J. A. Spitznagel, J. Nucl. Mater. 103&104 (1981) 1289–1304.

35. K. Farrell, P. J. Maziasz, E. H. Lee and L. K. Mansur, Rad. Eff. 78 (1983) 277–295.

36. P. J. Maziasz, ORNL-6121, Oak Ridge National Laboratory, 1985.

37. R. F. Mattas, F. A. Garner, M. L. Grossbeck, P. J. Maziasz, G. R. Odette, and R. E. Stoller, J. Nucl. Mater. 122&123 (1984) 230–235.

38. M. A. Abdow, et al., Blanket Comparison and Selection Study, ANL/FPP-83-1, Argonne National Laboratory, 1983.

39. L. K. Mansur, A. F. Rowcliffe, M. L. Grossbeck, and R. E. Stoller, Damage Analysis and Fundamental Studies Quarterly Progress Report, DOE/ER-0046/22, August, 1985, 13–23.

40. G. R. Odette, Damage Analysis and Fundamental Studies Quarterly Progress Report, DOE/ER-0046/21, May, 1985, 23–33.

## FIGURE CAPTIONS

Fig. 1. Comparison of model predictions and fast reactor swelling data (21,22).

Fig. 2. Comparison of model predictions and network dislocation density measurements (20,23).

Fig. 3. Comparison of model predictions of peak faulted loop density and fast reactor data (18,24–27).

Fig. 4. Influence of interstitial migration energy ($E_i^m$) on model predictions. Base case $E_i^m = 1.85$.

Fig. 5. Comparison of model predictions of faulted loop density using constant faulted loop/interstitial bias ($Z_i^\ell = 1.5$) and a size dependent bias (32).

Fig. 6. Model predictions of swelling and network dislocation density for fusion at 50 and 100 dpa. Base case is from fast reactor calibration. $p = 0.5$.

Fig. 7. Cavity density influence on model predictions for fusion. Base case is from fast reactor calibration.

ORNL-DWG 85-16844

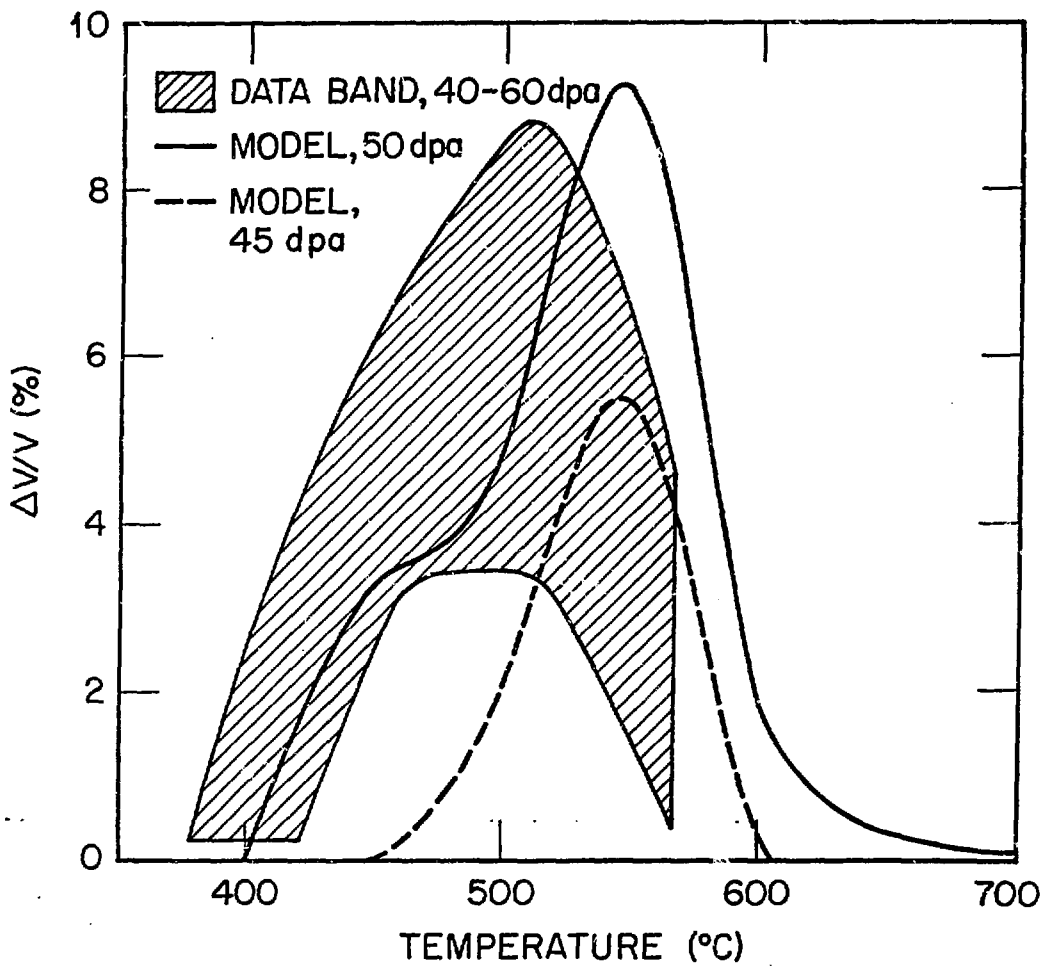


Stoller & Odette - M238

Fig. 1a

ORNL-DWG 85-16845

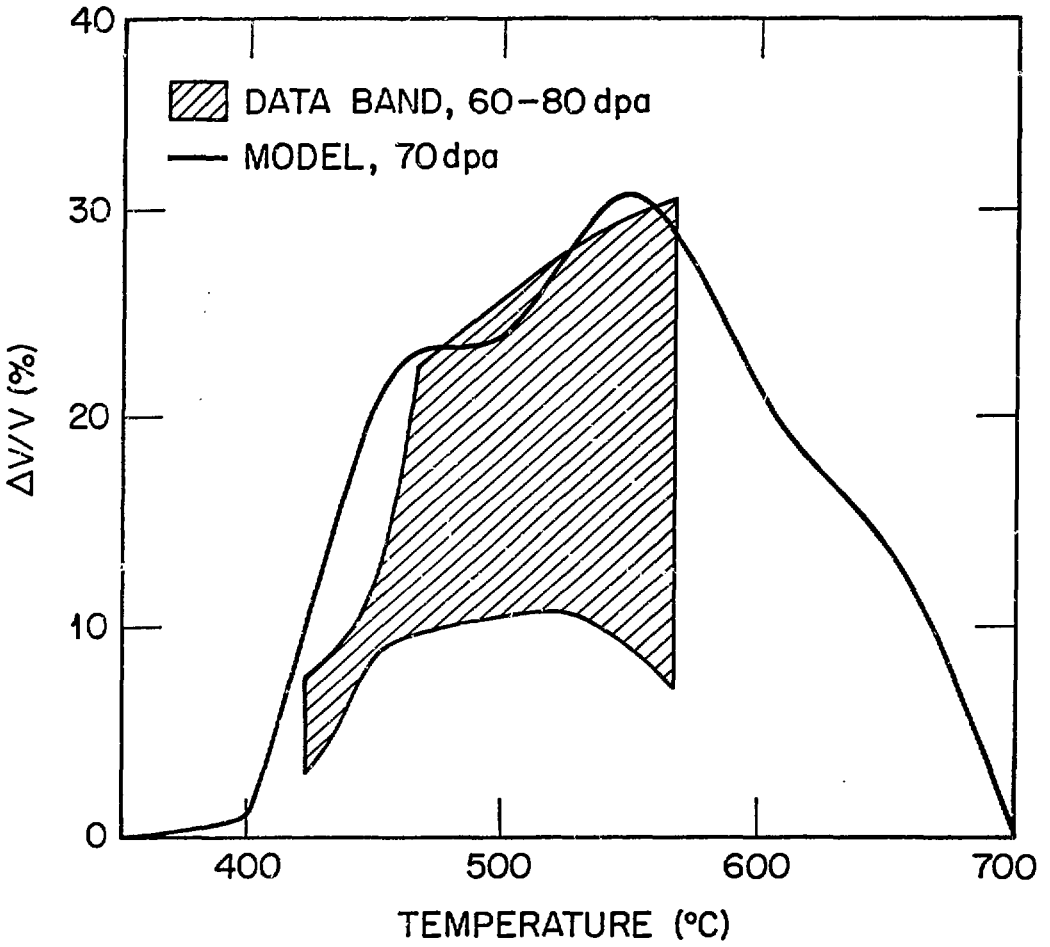


Stoller & Odette - M238

Fig. 1b

ORNL-DWG 85-16843R

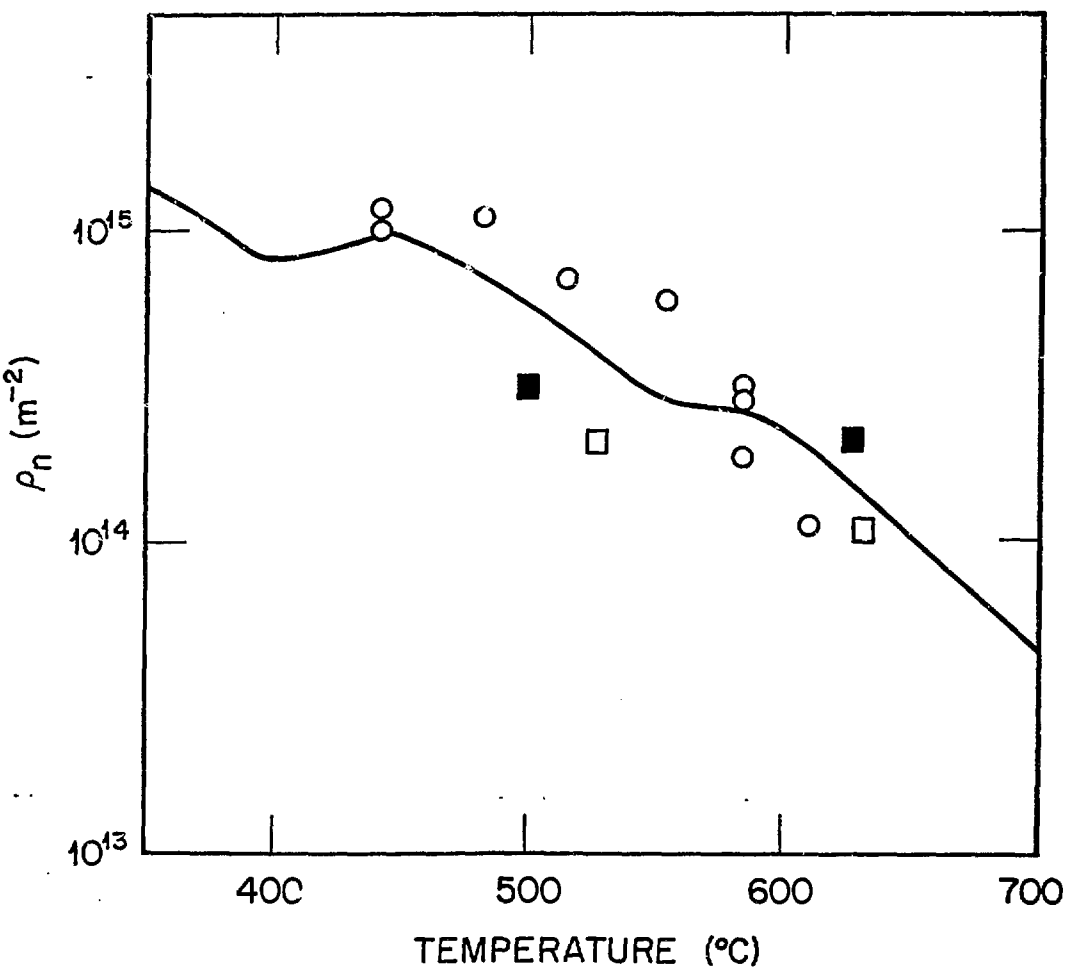


■ 8.4 dpa
□ 36 dpa
} PJM (DOE/ER-0045/7, 1981)

○ 29-40 dpa JIB, et al. (Rad. Effects in Breeder Reactor Structural Materials, 1977)

—— MODEL, 40 dpa

Stoller and Odette
M 258
Fig. 2

ORNL-DWG 85-17824R

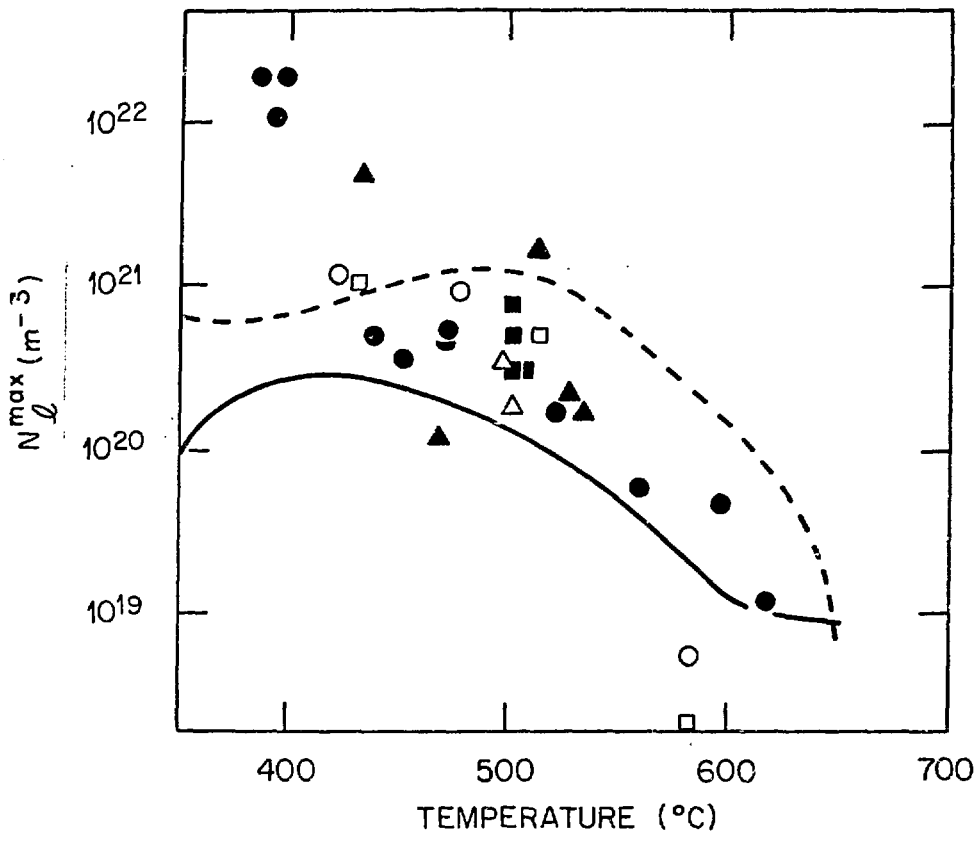


——— MODEL, $\rho_n(0) = 3 \times 10^{15}$ $m^{-2}$

– – – MODEL, $\rho_n(0) = 3 \times 10^{13}$ $m^{-2}$

● HRB AND JLS (JNM 46), SA 316

▲ PJB, BEL AND DAS (JNM 67), SA 316

○ HRB (JNM 57), CW 316

△ HRB, FAG AND GLG (JNM 66), CW 316

■ HRB, FAG AND GLG (JNM 66), SA 316

□ HEB AND JOS (ASTM STP 529), SA 316

Stoller and Odette
M 238
Fig. 3

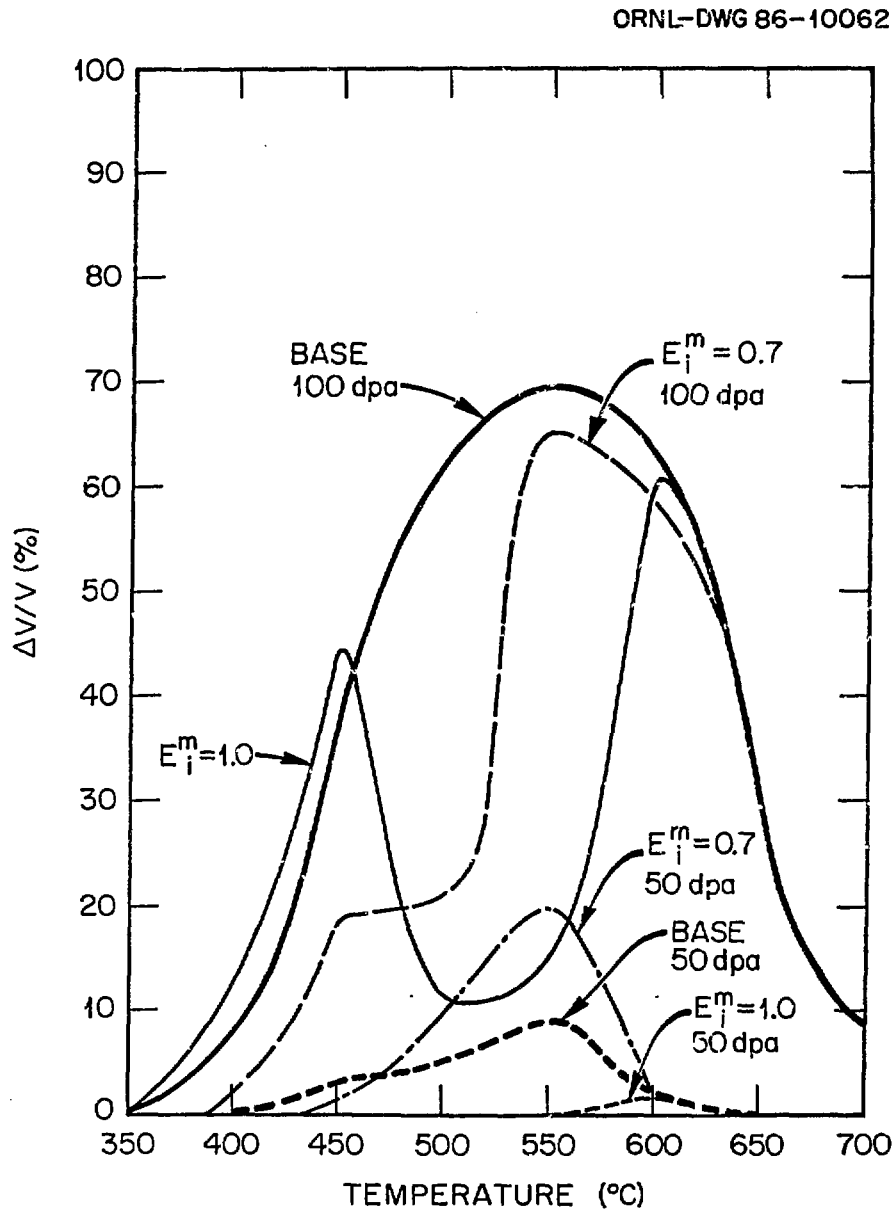


Stoller and Odette
M 258
Fig. 4a

ORNL-DWG 86-10063

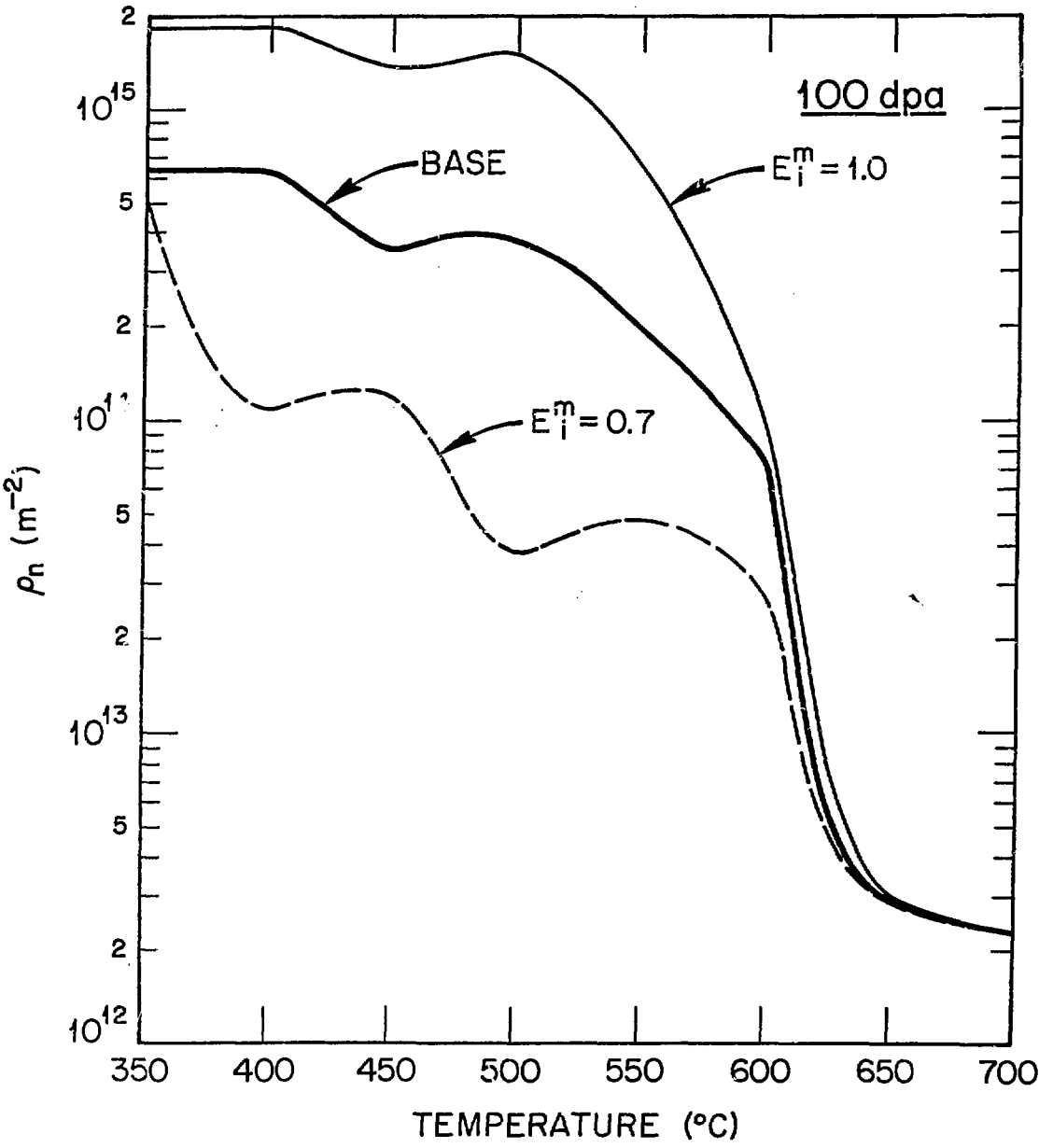


Stoller and Odette
M 258
Fig. 4b

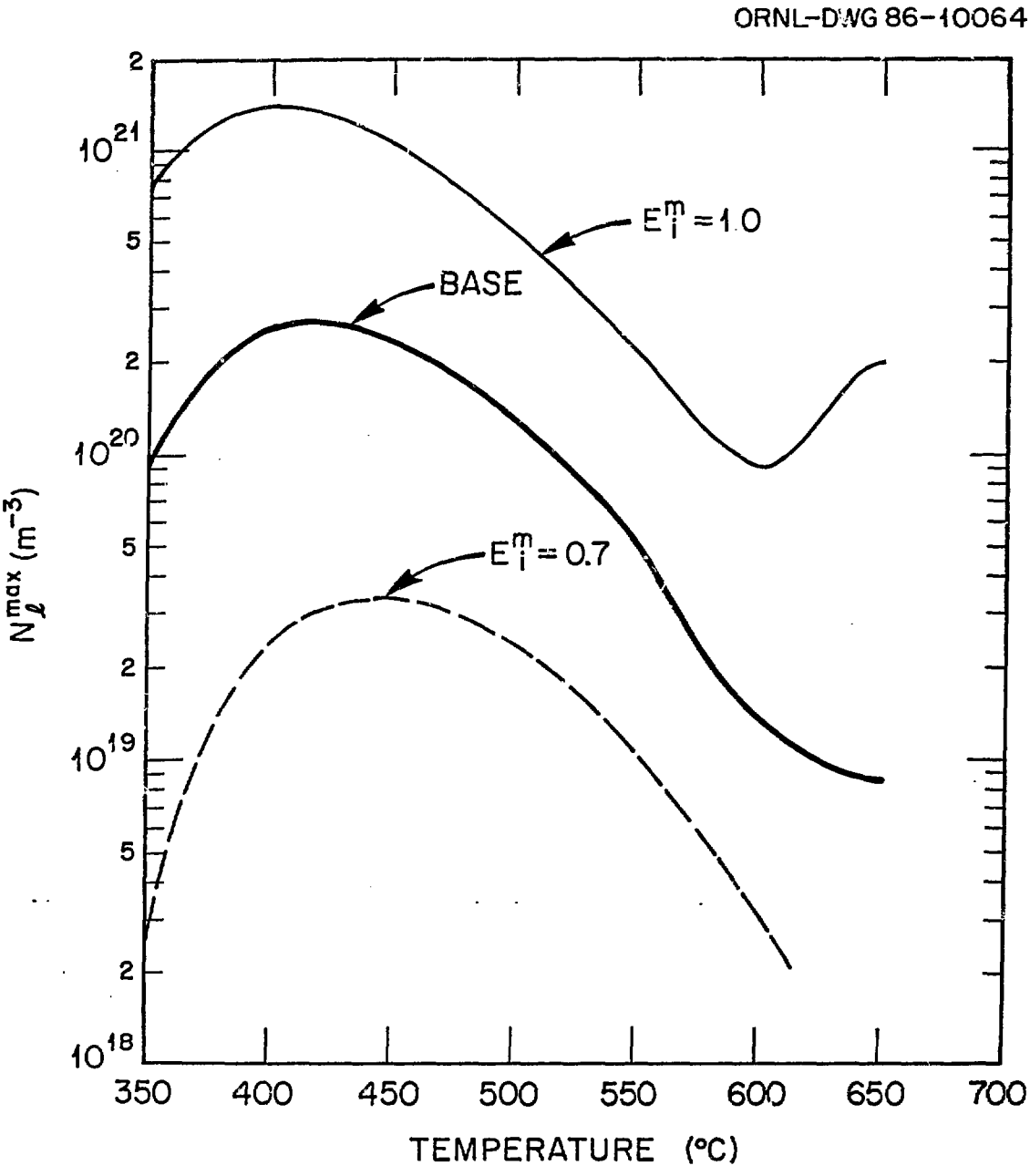


Stoller and Odette
M 258
Fig. 4c

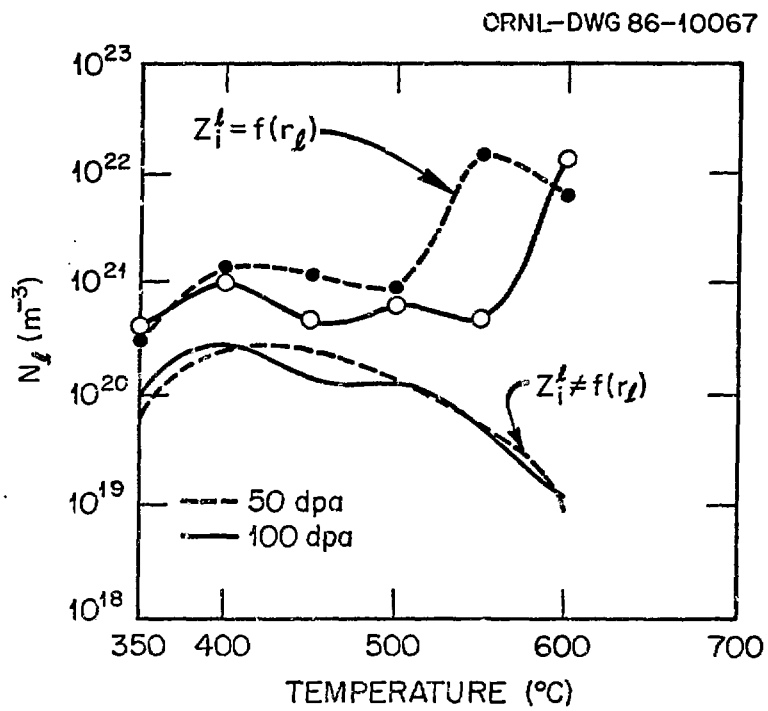


Stoller and Odette
M 238
Fig. 5a

ORNL-DWG 86-10068

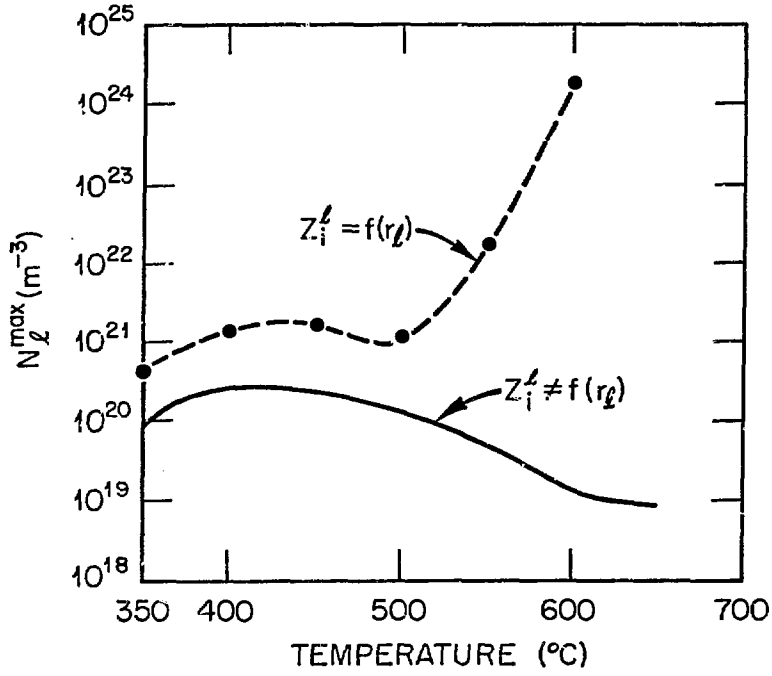


Stoller and Odette
M 238
Fig. 5b

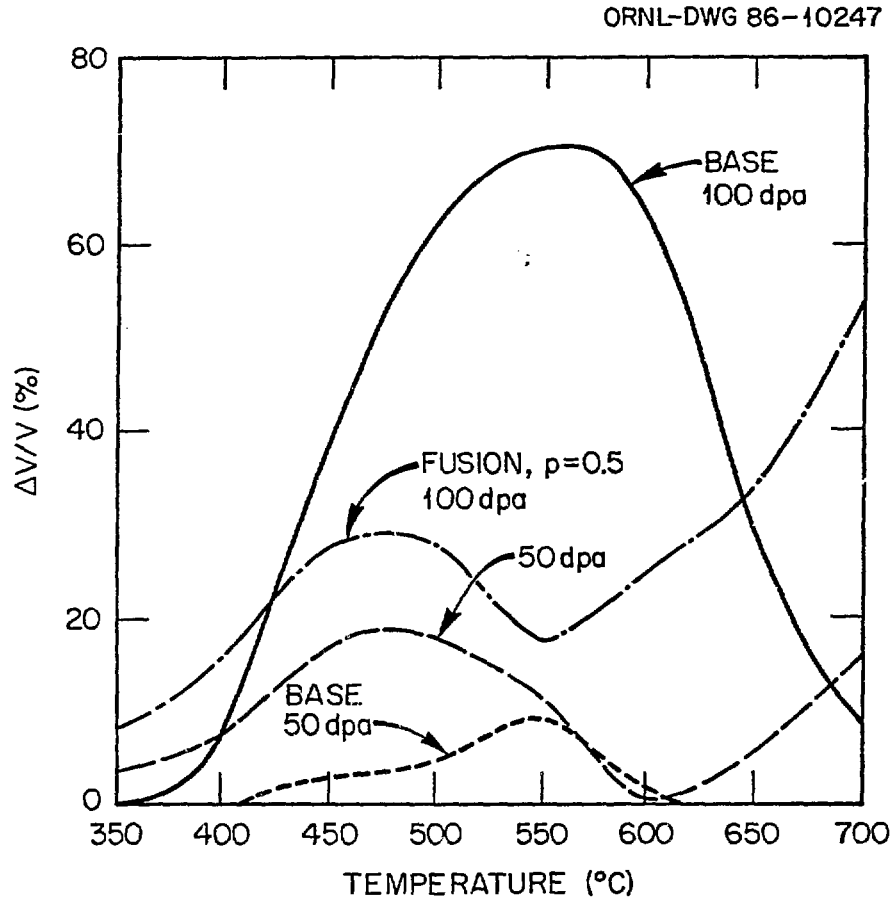


Stoller and Odette
M 238
Fig. 6a

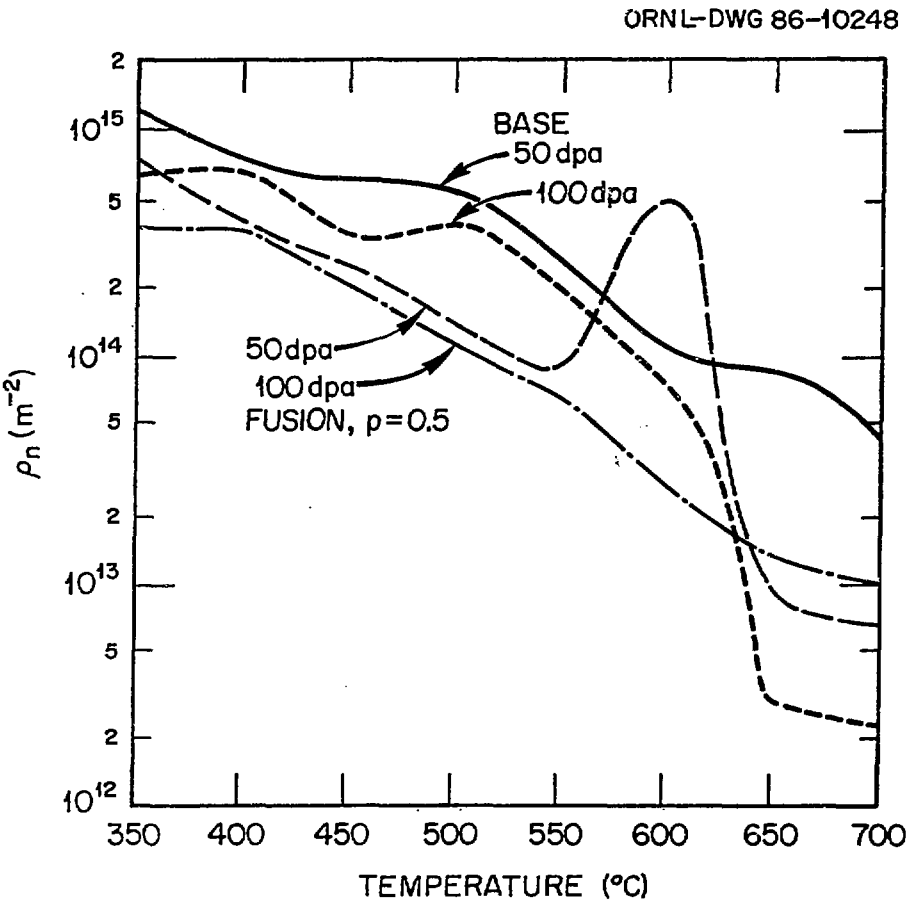


Stoller and Odette
M 258
Fig. 6b

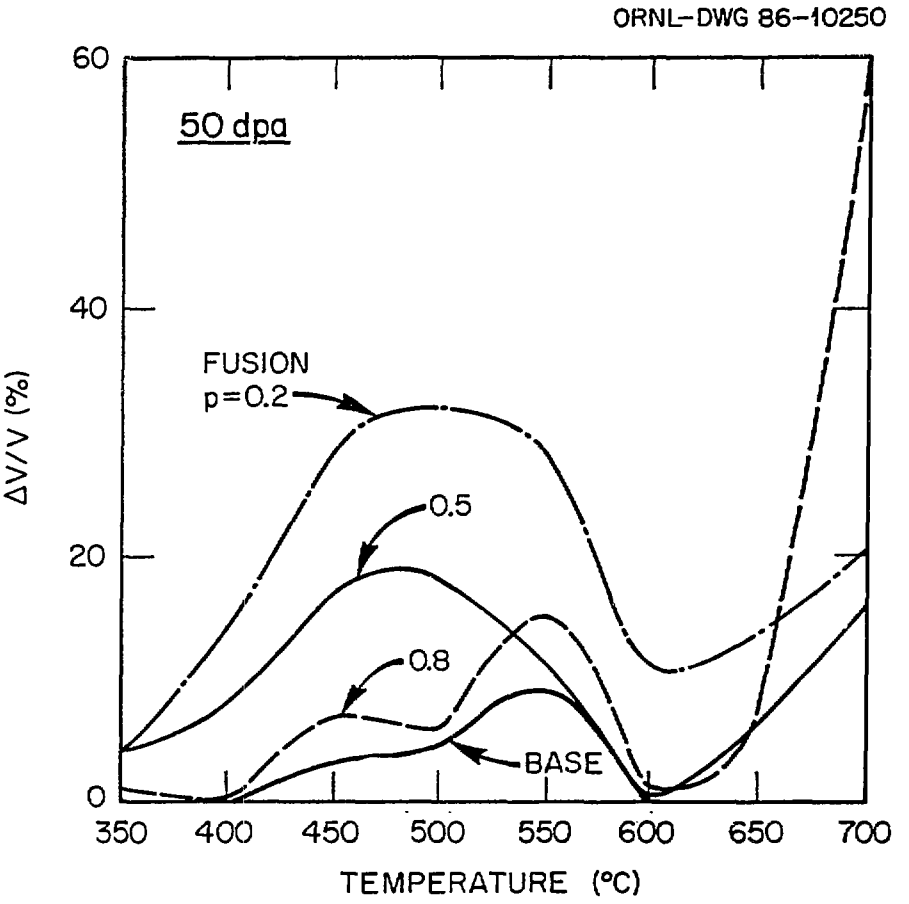


Stoller and Odette
M 258
Fig. 7a

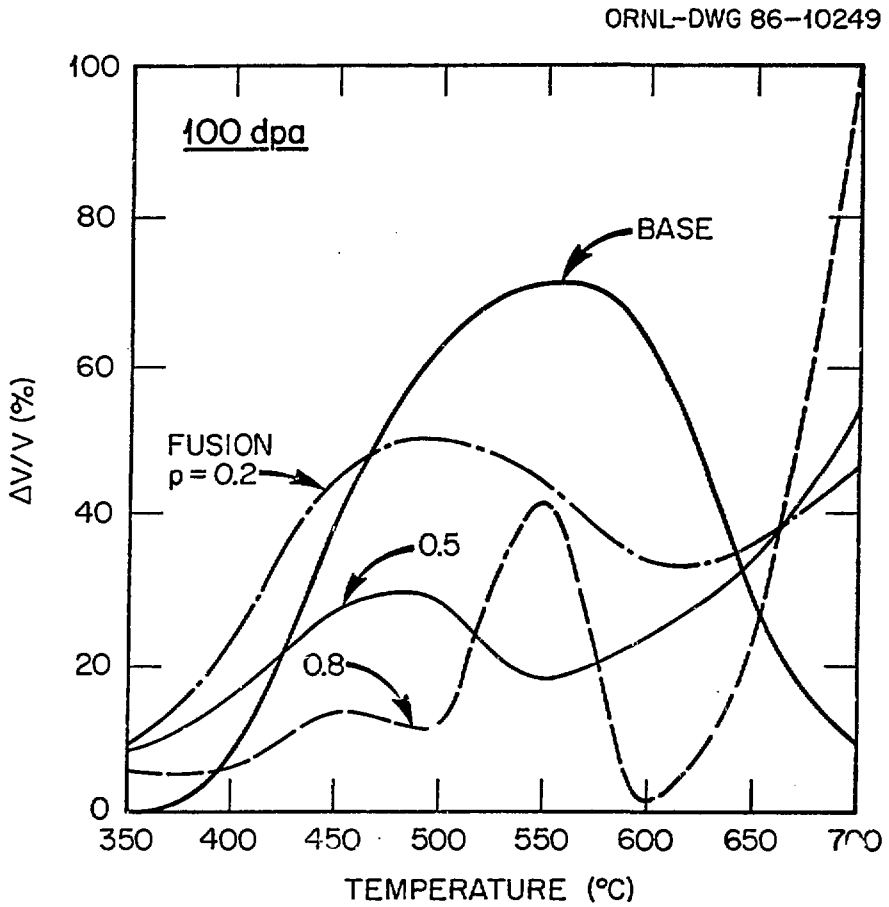


Stoller and Odette
M 238
Fig. 7b